where the weighted emissivity $\tilde{\epsilon}$ is given by

$$\tilde{\epsilon}(z,z_1) = \sum_i a_i^*(z,z_1) \frac{dB_i(z)}{dB(z)}$$

and $B(z)$ is integrated over all wave numbers [$\pi B(z) = \sigma T^4(z)$]. Of course, $\tilde{\epsilon}$ depends on the nature and concentration of the main emitters and on the pressure and temperature.

6.6 RADIATION BALANCE OF THE ATMOSPHERE

The heating or cooling of an atmospheric layer due to the change in net solar and terrestrial radiation with height can be calculated using the principle of conservation of energy. Let us consider a layer of the atmosphere between levels z and $z + \Delta z$ where the net vertical fluxes of radiation are $F(z)$ and $F(z + \Delta z)$, respectively. Then we find that

$$\rho c_p \Delta z \left(\frac{\partial T}{\partial t}\right)_{\text{rad}} = \frac{\partial F_{\text{net}}}{\partial z} \Delta z$$

or

$$\left(\frac{\partial T}{\partial t}\right)_{\text{rad}} = \frac{1}{\rho c_p} \frac{\partial F_{\text{net}}}{\partial z}, \tag{6.38}$$

where $F_{\text{net}} = F^{\uparrow} - F^{\downarrow}$.
If we express Eq. (6.38) in °C/day, we obtain

$$\left(\frac{\partial T}{\partial t}\right)_{\text{rad}} = \frac{8.64 \times 10^4}{\rho c_p} \frac{\partial F_{\text{net}}}{\partial z},$$

where the divergence is given in W m^{-3}, c_p in J kg^{-1} K^{-1}, and ρ in kg m^{-}

The application of this expression to the long-wave radiation component shows that this component generates a net cooling on the order of 2.5 °C per day. On the average, the heating of the atmosphere by absorption of solar radiation is only on the order of 0.5 °C/day, and therefore does not compensate for the cooling by long-wave radiation. The maintenance of a steady state in the atmosphere is only possible through the transfer of sensible heat (enthalpy) and latent heat (evaporation–condensation) from the earth's surface to the atmosphere.

In the daytime and with clear skies, the net radiation balance is dominated by the short-wave solar radiation but at night the balance is, of course, entirely due to the long-wave radiation. Because the concentrations of some of the absorbers (e.g., H_2O and O_3) vary strongly with height the solar and terrestrial radiation fluxes are also strongly height dependent. In general, in clear and calm nights the long-wave radiative flux increases with height, leading to a flux divergence and a cooling of the atmosphere.

Clouds have a strong effect on the transfer of long-wave radiation because they modify the emissivity of the atmosphere at certain wavelengths. Clouds are almost completely opaque for infrared radiation. They act as if they close the atmospheric window, preventing the escape of long-wave radiation into space. This effect is large enough to strongly influence the surface temperature. For example, under cloudy conditions the nocturnal temperature drop will be much reduced as compared with clear night conditions. Even the presence of a thin layer of cirrus clouds can be

enough to cause an increase in surface air temperature because of the additional long-wave radiation emitted by the clouds.

Manabe and Strickler (1964) used a simple one-dimensional climate model to study the contributions by H_2O, CO_2, and O_3 to the atmospheric heating and cooling rates (see Chap. 17). Their model was based on the radiative transfer equations given earlier in this chapter taking into consideration the main absorption bands of the absorbers. Their results for the case that the cloudiness is equal to the global mean value are shown in Fig. 6.7.

The troposphere shows a net radiative cooling mainly due to water vapor, which is compensated by the latent and sensible heating associated with moist convection. In the stratosphere, there is a strong heating due to the absorption of ultraviolet solar radiation by ozone and to a much smaller extent, due to the absorption of long-wave terrestrial radiation in the 9.6-μm band [see Fig. 6.2(b)]. We may note that the long-wave heating is only possible because of the low concentrations of O_3 in the troposphere. The cooling in the stratosphere is due to long-wave emission mainly by CO_2 and to a lesser extent by water vapor and ozone. In the one-dimensional model of Manabe and Strickler, the heating and cooling in the stratosphere compensate because the stratosphere is assumed to be in radiative equilibrium.

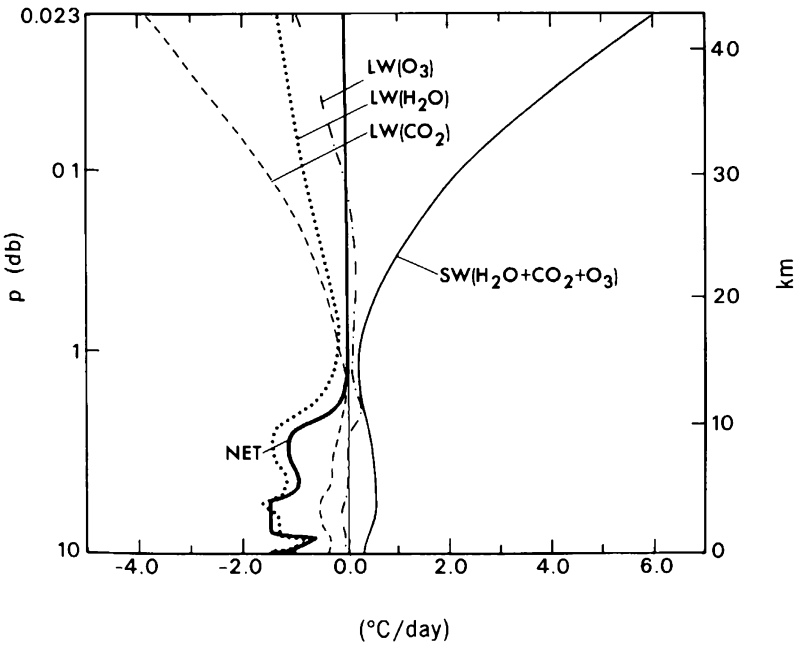

FIGURE 6.7. Vertical distributions of the computed rate of temperature change in the atmosphere for thermal equilibrium due to various absorbers. $LW(H_2O)$, $LW(CO_2)$, and $LW(O_3)$ show the rate of temperature change due to long-wave radiation emission and absorption by water vapor, CO_2, and O_3, respectively. $SW(H_2O + CO_2 + O_3)$ shows the rate of temperature change due to the absorption of solar radiation by these three gases. "Net" means the net rate of temperature change due to all components (adapted from Manabe and Strickler, 1964).

In the 8–12-μm region the atmosphere is almost transparent for long-wave terrestrial radiation, with the exception of the absorption at 9.6 μm by ozone [see Figs. 6.2(b) and 6.2(c)]. This region of the spectrum is therefore known as the atmospheric spectral window. It is also the range where the long-wave radiation for the atmosphere is a maximum [see Eq. (6.6)]. It is interesting to note that, through absorption in the spectral window, small increases of CO_2 or of other trace gases may have a large impact on the climate. In fact, Ramanathan *et al.* (1985) have brought attention to the fact that some minor trace gases, such as chlorofluorocarbons, methane (CH_4), and nitrous oxides (N_2O), also have absorption lines in the spectral window. The recent increase in the concentrations of these trace gases can lead to additional trapping of the radiation emitted by the earth's surface and thereby to heating of the troposphere and cooling of the stratosphere.

Several other studies have been made using observed distributions of the absorbers in the atmosphere as, e.g., the study by Dopplick (1979). His results show a net radiative cooling throughout the year at almost all latitudes in the troposphere. However, in the stratosphere he finds heating at low latitudes and cooling at mid and high latitudes. All the studies mentioned so far are limited by an incomplete knowledge of the concentrations of the various absorbers in the upper troposphere and stratosphere and by the difficulties of incorporating the effects of clouds.

Most of the atmospheric gases have bands in the microwave region of the spectrum. These bands are not important in the transfer of infrared radiation in the atmosphere, because in the microwave region the thermal radiative fluxes are very small. However, they are being used to infer the vertical profiles of temperature, moisture, and liquid water in clouds through remote sensing from satellites.

6.7 RADIATION BALANCE AT THE EARTH'S SURFACE

The net flux of radiation at the earth's surface results from a balance between the solar and terrestrial radiation fluxes:

$$F_{\text{rad}}^{\text{sfc}} = F_{\text{SW}} + F_{\text{LW}}.$$

The short-wave and long-wave radiation balance can be expressed by

$$F_{\text{SW}} = F_{\text{SW}}^{\downarrow} - F_{\text{SW}}^{\uparrow}$$

and

$$F_{\text{LW}} = F_{\text{LW}}^{\downarrow} - F_{\text{LW}}^{\uparrow}.$$

Therefore, the overall radiation balance becomes

$$F_{\text{rad}}^{\text{sfc}} = F_{\text{SW}}^{\downarrow} - F_{\text{SW}}^{\uparrow} + F_{\text{LW}}^{\downarrow} - F_{\text{LW}}^{\uparrow},$$

where the downward and upward arrows denote the incoming and outgoing radiation components, respectively.

The incident solar radiation $F_{\text{SW}}^{\downarrow}$ is the sum of the direct and diffuse solar radiation. It has a pronounced diurnal and seasonal variation, and is also strongly affected by clouds. The outgoing short-wave solar radiation is the part reflected by the surface $F_{\text{SW}}^{\uparrow} = A_{\text{sfc}} F_{\text{SW}}^{\downarrow}$, where A_{sfc} is the surface albedo so that the net short-wave radiation is

$$F_{\text{SW}} = (1 - A_{\text{sfc}}) F_{\text{SW}}^{\downarrow}.$$

The incoming long-wave radiation $F^{\downarrow}_{LW}$ comes from the atmosphere and depends on the vertical temperature profile, the clouds, and the vertical distribution of the absorbers. It does not show a significant diurnal variation. The outgoing long-wave radiation $F^{\uparrow}_{LW}$ is given by the Stefan–Boltzmann law, assuming a given emissivity ϵ for the earth's surface. As expected, it follows the diurnal cycle in surface temperature with a maximum value in the early afternoon and a minimum value in the early morning. The incoming and outgoing long-wave radiation components have the same order of magnitude so that the net long-wave radiation flux is small compared to the net solar flux. However, it becomes important at night when $F_{SW} = 0$. Usually $|F^{\downarrow}_{LW}| < |F^{\uparrow}_{LW}|$ implying a long-wave radiative cooling of the surface.

The net radiation flux at the surface is then given by

$$F^{sfc}_{rad} = F^{\downarrow}_{SW}(1 - A_{sfc}) - \epsilon\sigma T^{4}_{sfc} + F^{\downarrow}_{LW}. \tag{6.39}$$

This net radiation heats the surface.

The infrared radiation emitted by the surface $\epsilon\sigma T^{4}_{sfc}$ is strongly absorbed by water vapor and carbon dioxide in the atmosphere. In turn, the atmosphere will re-emit the absorbed energy both upward and downward. The downward component will be absorbed by the earth's surface and heat it. Thus, the temperature of the earth will be higher than it would be if the atmosphere were transparent for the long-wave radiation. This so-called greenhouse effect was mentioned earlier in Chap. 2.

The observed world-wide increase in the concentrations of CO_2 and other trace gases in the atmosphere must enhance the greenhouse effect and may lead to a net increase in surface temperature over the earth.

The main part of the energy absorbed at the surface is used to evaporate water, another part is lost to the atmosphere as sensible heat, and a smaller part is lost to the underlying layers or used to melt snow and ice. Thus, there are essentially four types of energy fluxes at the earth's surface. They are the net radiation flux F_{rad}, the (direct) sensible heat flux $F^{\uparrow}_{SH}$, the (indirect) latent heat flux $F^{\uparrow}_{LH}$, and the heat flux into the subsurface layers $F^{\downarrow}_{G}$. Under steady conditions the balance equation for the energy is given by

$$F^{sfc}_{rad} - F^{\uparrow}_{SH} - F^{\uparrow}_{LH} - F^{\downarrow}_{G} - F_{M} = 0, \tag{6.40}$$

where F_M is the energy involved in melting snow and ice or in freezing water. This energy budget equation will be analyzed in more detail in Sec. 10.2.

6.8 OBSERVED RADIATION BALANCE

As is well known, the radiational energy of the sun constitutes the basic driving force for the atmospheric and oceanic general circulations. Thus, the most important external factor for the earth's climate is the total incoming solar radiation. As mentioned before in Sec. 6.3, the incoming solar radiation is characterized by the solar constant, the obliquity, the eccentricity, and the longitude of perihelion for the earth's orbit around the sun. Variations in these astronomical factors may be closely linked to observed variations in the earth's climate at time scales of thousands of years and longer (see Figs. 2.5 and 2.7). However, they do not seem important at the decadal time scale which we are concerned with in this book.

6.8.1 Radiation balance of the earth

One of the most important scientific contributions of meteorological satellites has been the measurement of the radiation budget at the top of the atmosphere. This involves measuring both the solar short-wave input and the terrestrial long-wave output components. Measurements of the planetary albedo combined with the known impinging solar radiation at the top of the atmosphere supply the necessary information on the first component of the radiation budget, the net solar input. Uncertainties in the present albedo values are related to inadequate diurnal sampling and incomplete knowledge of how to extrapolate from measurements at one zenith angle to full half-sphere values. The second component of the radiation budget involves measuring the long-wave, terrestrial radiation. Less uncertainty seems to be involved in this determination, except for effects associated with the diurnal cycle in cloudiness.

By and large, the earth as a whole is in radiative equilibrium averaged over a period of several years. In other words, as much energy must be leaving the system in the form of long-wave radiation as is entering in the form of short-wave radiation:

$$F_{TA} = \int_{top} (1 - A) F^{\downarrow}_{SW}\, ds - \int_{top} F^{\uparrow}_{LW}\, ds \simeq 0, \tag{6.41}$$

where F_{TA} = net flux of radiation at the top of the atmosphere, $F^{\downarrow}_{SW}$ = incoming solar flux, and $F^{\uparrow}_{LW}$ = long-wave flux to space.

Since the average albedo of the earth is on the order of 30%, an amount of solar radiation given by

$$(\pi R^2/4\pi R^2)\ (1 - A)\ S = 238 \text{ W m} \tag{6.42}$$

is absorbed in the atmosphere and oceans, and later re-emitted as long-wave terrestrial radiation, where the solar constant $S \simeq 1360$ W m^{-2} The value of 238 W m^{-2} is a useful reference number for our later studies of the radiational energy available for the atmospheric and oceanic energetics.

Assuming that there is a balance between the amount of solar energy received and the amount of energy emitted by the earth as a whole and that the earth radiates as a black body, we can compute the so-called radiative equilibrium temperature T_e of the earth from the Stefan–Boltzmann law (6.5) so that

$$\sigma T_e^4 = 238 \text{ W m}$$

or

$$T_e = 255 \text{ K or } -18\ ^{\circ}\text{C}.$$

However, Eq. (6.39) shows that due to the existence of the atmosphere with gases that absorb and emit the long-wave radiation, the surface temperature of the earth T_{sfc} is greater than the effective emission temperature T_e. Thus,

$$T_{sfc} = T_e + \Delta T, \tag{6.43}$$

where ΔT represents the atmospheric greenhouse effect on the surface temperature. Since the mean surface temperature of the earth is 288 K, the greenhouse effect due to the existence of the atmosphere is $\Delta T = 33$ K.

If $\overline{F}_{TA} \neq 0$, the earth would be subject to cooling or heating. However, as far as we can tell, in view of the present uncertainties in the data (~ 10 W m^{-2}), this does not seem to be the case. A possible exception is the global surface heating associated with the observed increases in CO_2 and other trace gases that is generally expected to become noticeable in the near future. For example, an annual excess of 1% of ab-

sorbed over emitted flux ($\overline{F}_{TA} = 2.38$ W m^{-2}) would be equivalent to a heating of about 7 K of the entire atmosphere or a heating of 1 °C of the top 25 m of the world oceans if the excess were maintained during the period of one year.* Such an imbalance in the climatic system should be detectable from the global atmospheric and oceanic temperature records. We may note that the heating due to geothermal processes can be neglected because it is estimated to be on the order of 0.06 W m^{-2}, or less than 0.03% of the absorbed solar radiation.

The next question is whether the earth is also in radiative equilibrium averaged over shorter periods, i.e., over the period of a month or season. First of all one has to consider the annual variation in the earth–sun distance from 0.983 AU in January to 1.017 AU in July. Assuming no annual variation in the global albedo, one would expect a difference in the absorbed radiation inversely proportional to the earth–sun distance squared [see Eq. (6.16)]. Thus, one would expect a difference in solar input of $238/(0.983)^2 - 238/(1.0167)^2 = 16.1$ W m^{-2} between January and July equivalent with a value of about 7% of the net available radiational energy.

Both the computed and the actually observed annual variations are shown in Fig. 6.8. Differences between the two curves are caused by variations in the global albedo. The passage of the sun twice a year over the relatively dark tropics during the time of the equinoxes is connected with a greater absorption of radiation by the earth. On the other hand, during the solstices more reflection of sunlight and less absorption occurs since the sun then illuminates the ice-covered polar caps. The combined effects lead to a semiannual variation in the net radiation curve. Furthermore, there is an asymmetry in the response of the two hemispheres caused by the large seasonal variation in the area covered by snow in the Northern Hemisphere compared with the relatively minor variations inthe Southern Hemisphere (see Fig. 9.4). Besides snow and ice, changes in cloudiness (see Fig. 7.29) and vegetation will also affect the planetary albedo. Nevertheless, the variation of the incident solar radiation at the top of the atmosphere is mainly due to the variation in the earth–sun distance.

Offhand, one might expect a compensation through stronger long-wave cooling of the earth in January than July to ensure radiative equilibrium at the monthly time scale. However, satellite data show that this is not the case. In fact, infrared cooling is observed to be stronger in July than in January, as illustrated in Fig. 6.9. This process may be classified as a positive feedback effect of the earth. The reason lies in the asymmetry of the two hemispheres. The Northern Hemisphere atmosphere is subject to much greater seasonal variations in its temperature than the Southern Hemisphere atmosphere because the major continents are located in the Northern Hemisphere. Therefore, the seasonal variation in global temperature tends to follow the northern seasons leading to a greater global heat loss in July than in January. Cloudiness will also play a role but it is certainly less dominant than temperature.

Combining the estimates of the gain in solar radiation and the loss in terrestrial radiation in Fig. 6.9, we find that the net radiation flux at the top of the atmosphere undergoes an annual cycle with January–July differences of about 25 W m^{-2} We may speculate that if the major continents were moved from their present position in

*The global excess in radiation after one year would be 5.12×10^{14} m$^2\times2.38$ W m$^{-2}\times3.15\times10^7$ s $= 3.84\times10^{22}$ J. Since the area of the world ocean is 3.61×10^{14} m^2, the specific heat of water is 4200 J kg^{-1} °C^{-1} and the density of sea water is about 10^3 kg m^{-3}, an equivalent average heating of 1 °C would take place for an ocean layer of 3.84×10^{22} J/$(3.61\times10^{14}$ m$^2\times4200$ J kg^{-1} °C$^{-1}\times10^3$ kg m$^{-3}\times1$°C$) = 3.84\times10^{22}/(15.1\times10^{20})$ m$\approx$25 m.

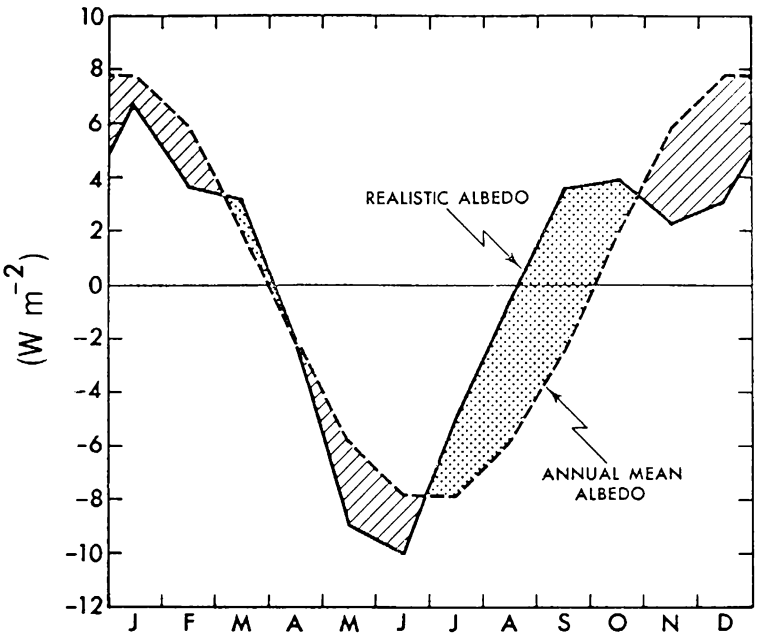

FIGURE 6.8. Seasonal variation of the net incoming solar radiation as observed by satellites at the top of the atmosphere (solid curve) and of the computed solar radiation assuming an idealized annual-mean value of the albedo throughout the year (dashed curve). The annual-mean value of the incoming solar radiation (241 W m ^{2}) has been subtracted out. The differences between the two curves must be due to seasonal differences in cloudiness and snow and ice cover, affecting the albedo of the earth–atmosphere system.

the Northern to the Southern Hemisphere, the annual cycle in global radiation would be drastically changed and radiative equilibrium might prevail over the course of a year.*

With improved satellite observations of the solar constant, the global albedo and the global outgoing long-wave flux new opportunities will arise in the near future to study the presently unknown, but possibly significant, global imbalances that might occur at time scales from months to years. Conceivably such imbalances would be important in interannual climatic fluctuations and longer-term climatic changes.

Finally, we should add that the observed excess or deficit in radiative heating of the earth during the course of a normal year (as shown in Fig. 6.9) has to show up as an increased or decreased energy level of the earth itself (Ellis *et al.*, 1978). We will come back to this issue in Chap. 13 (see Fig. 13.22).

*We should note that the more recent Nimbus and ERBE data (e.g., Weare and Soong, 1990) confirm the short-wave radiation values shown in Fig. 6.9, but give a reduced annual range on the order of 8 W m $^{-2}$ for the global long-wave flux values.

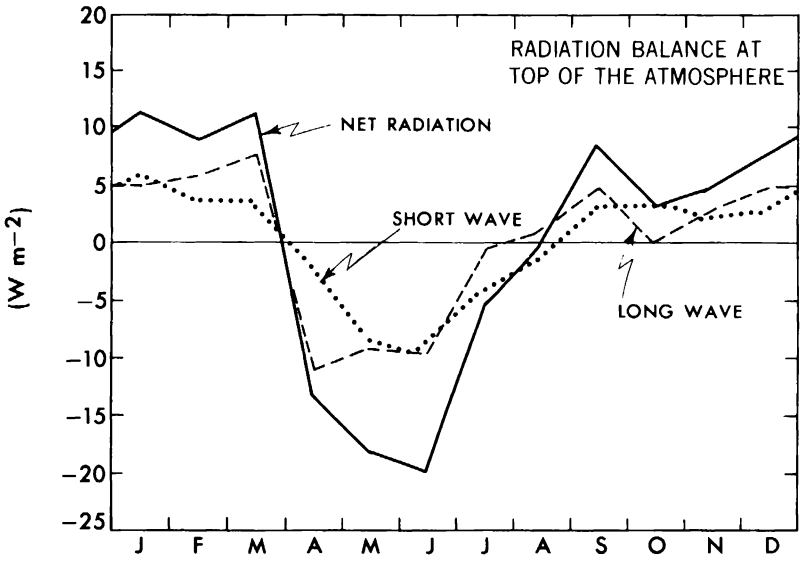

FIGURE 6.9. Radiation balance at the top of the atmosphere for the solar (short-wave), terrestrial (long-wave), and net radiation components as a function of month of the year. Shown are the departures from the annual-mean values.

6.8.2 Global distribution of the radiation balance

We will now discuss a series of radiation maps (Figs. 6.10 and 6.11) that are based on satellite observations reduced by Campbell and Vonder Haar (1980).

The incoming solar radiation that becomes available for driving the climatic system is strongly modulated by the albedo. Figure 6.10(a) shows the distribution of the albedo over the globe with values increasing monotonically from the equatorial regions where it has the lowest values (on the order of 20% and less) to the polar regions where the values are the largest (ranging between 60% and 95%). The maxima observed in the polar regions are mainly associated with the snow cover and the high angle of incidence of the solar radiation. The minimum values in the intertropical zone are located over the oceans with somewhat higher values over the subtropical continents, in general agreement with the corresponding cloud distributions (see Fig. 7.28). Worth mentioning is the high albedo over the Sahara desert where the cloudiness attains a minimum. During December–February (not shown) the subtropical minima in the albedo are mainly located in the Southern Hemisphere and during June–August they shift northward into the Northern Hemisphere.

The available solar radiation, given by $(1 - A)F^{\downarrow}_{\mathrm{SW}}$, is presented in Fig. 6.10(b) for annual-mean conditions. As expected, the figure shows that the available solar radiation is negatively correlated with the albedo. The highest values of about 350 W m^{-2} tend to occur over the intertropical oceans, decreasing almost monotonically to values less than 100 W m^{-2} at the poles.

The global distribution of the infrared radiation emitted by the earth is shown in Fig. 6.10(c) for the annual-mean case. The highest values (on the order of 270–280

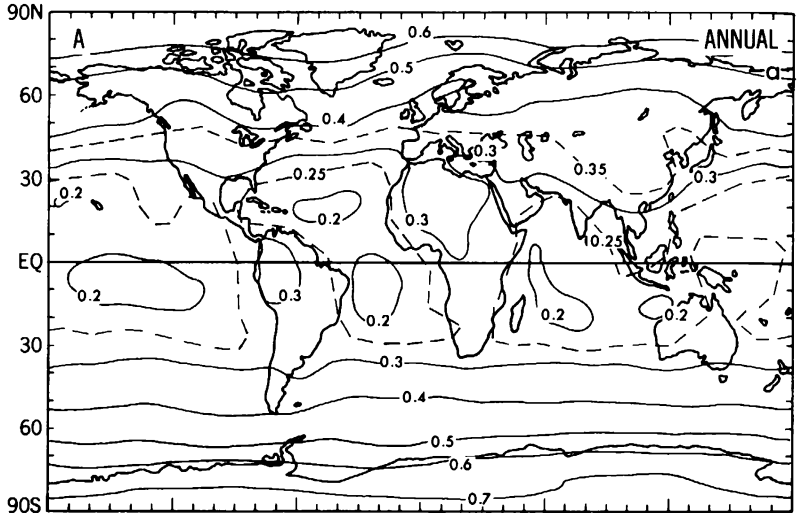

FIGURE 6.10a

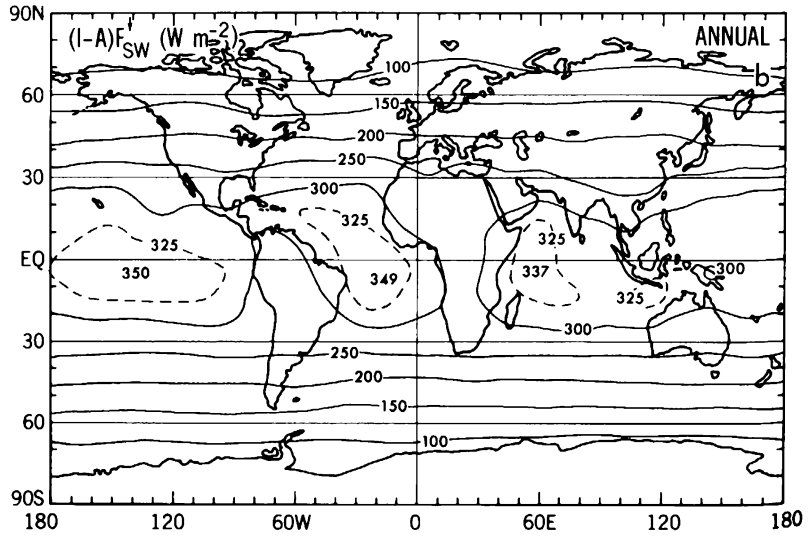

FIGURE 6.10b

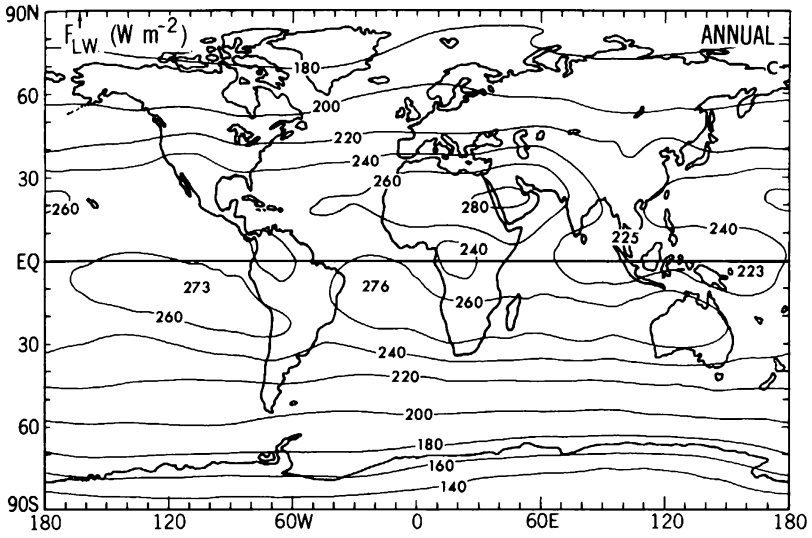

FIGURE 6.10. Global distributions of the albedo A (a), absorbed solar radiation $(1 - A)F^{\downarrow}_{SW}$ (b), and outgoing terrestrial radiation $F^{\uparrow}_{LW}$ (c) for annual-mean conditions (based on data from Campbell and Vonder Haar, 1980).

W m^{-2}) are observed over the subtropical latitudes decreasing gradually towards the poles where they reach values of 160 W m^{-2} and less. The seasonal distributions (not presented here) show similar patterns with two double maxima straddling the equator. The tropical values tend to be negatively correlated with the cloud distribution. Thus, when high clouds are present the emission temperatures are lower leading to lower values of the emitted radiation (Stefan–Boltzmann law). The global distribution of emitted radiation is very different from that of the absorbed solar radiation which shows much stronger latitudinal gradients.

Finally, Fig. 6.11 shows the net radiation at the top of the atmosphere for the year and the northern winter and summer seasons. The annual picture basically shows a zonal pattern with energy input ranging from about 60 to 70 W m^{-2} near the equator and energy losses of about 100 W m^{-2} near the south pole and 120 W m^{-2} near the north pole. For the year as a whole, Fig. 6.11(a) shows that the ocean regions generally gain more energy than the land regions, pointing to the need for a net annual transport of energy by the atmospheric circulation from the oceans into the land. Of particular interest is the strong negative anomaly over the North African desert, requiring an appreciable influx of atmospheric energy or, in other words, requiring adiabatic heating by compression of the air to compensate for the radiational cooling. This is mainly a summer phenomenon.

Predominant zonality of the net incoming radiation is clear in the winter hemispheres in Figs. 6.11(b) and 6.11(c). The summer hemisphere patterns are broken up with minima of net radiation over the continents and maxima over the oceans. The reasons for these continent–ocean differences are that the values of the surface albedo are larger over land than over water leading to more reflection of solar radiation over land, and that the infrared radiation losses during summer tend to be greater over

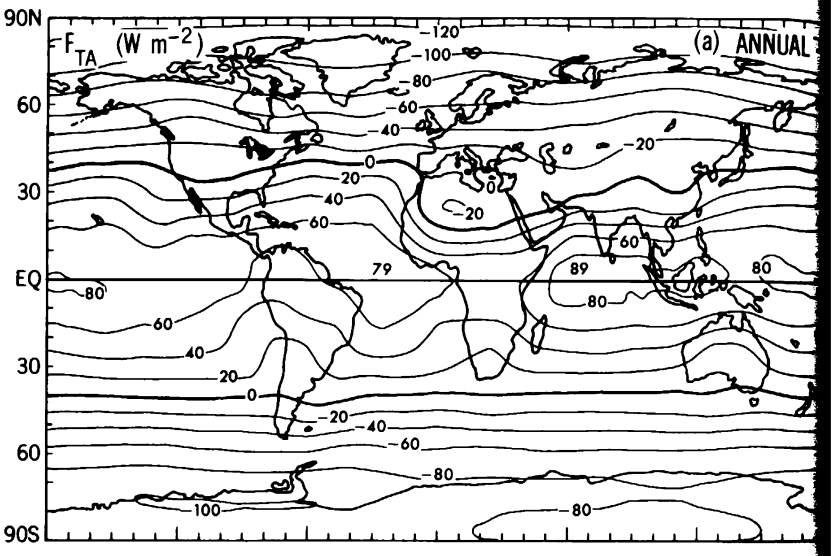

FIGURE 6.11a

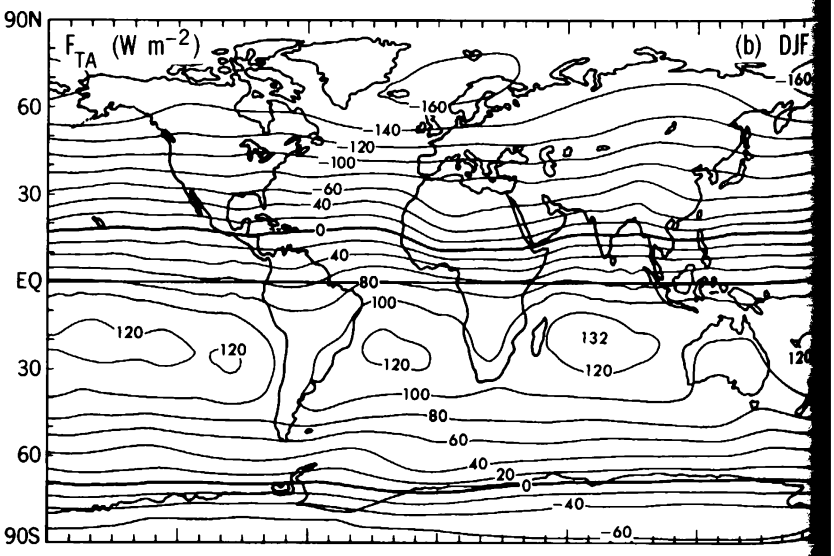

FIGURE 6.11b

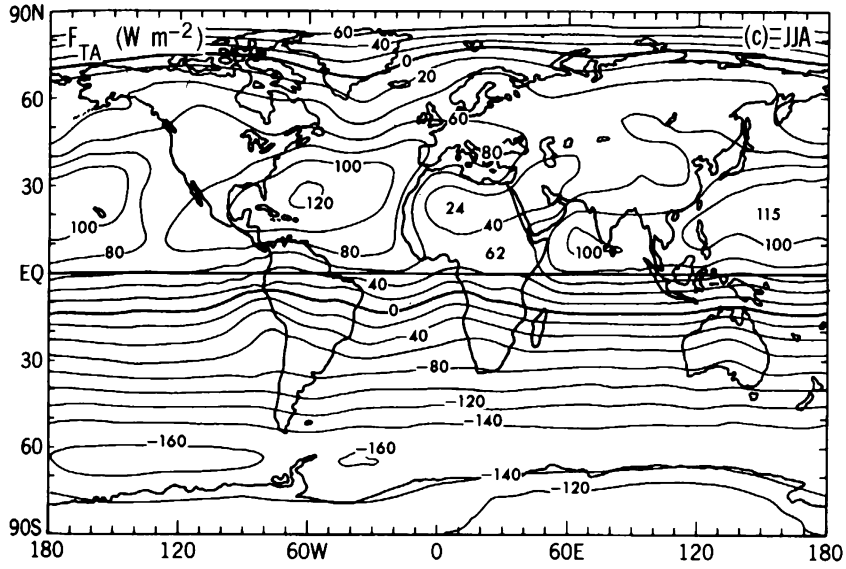

FIGURE 6.11. Global distributions of the net incoming radiation F_{TA} at the top of the atmosphere for annual (a), northern winter (b), and northern summer (c) mean conditions in W m (based on data from Campbell and Vonder Haar, 1980).

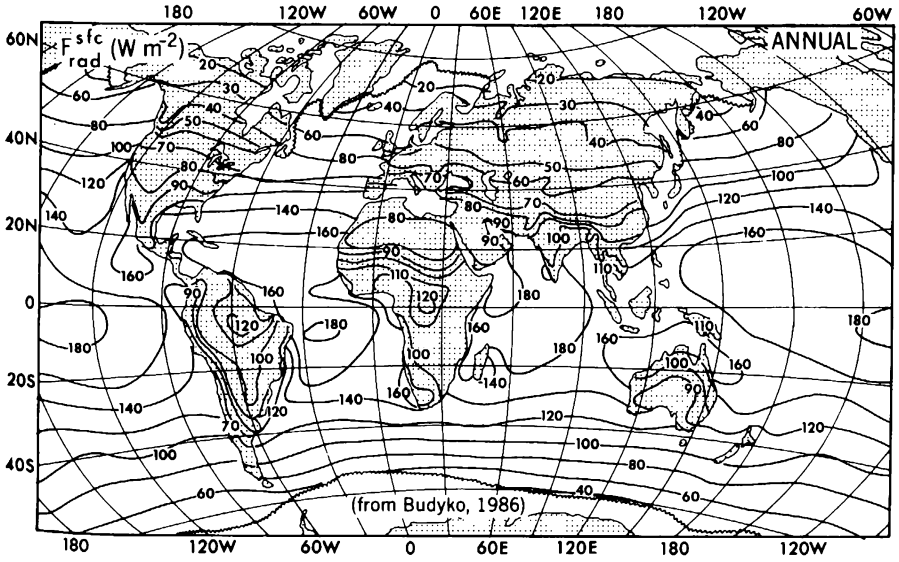

FIGURE 6.12. Global distribution of the net downward radiation flux F^{sfc}_{rad} at the earth's surface for annual-mean conditions in W m^{-2}. The annual-mean ice boundary is indicated by a wiggly line. Above the ice in winter F^{sfc}_{rad} can be negative (i.e., upward) (after Budyko, 1986).

the relatively warm continents than over the cool oceans. Much of the excess of summer radiation over the oceans is absorbed in the oceans themselves.

By subtracting estimates of the seasonal heat storage in the oceans and in the overlying atmosphere from the net radiation values, Campbell and Vonder Haar (1983) were able to determine the need for a substantial atmospheric transport of energy from the land to the ocean regions during summer, and from the oceans to the land during winter.

The strongest north–south energy fluxes in the atmosphere should occur in the winter hemisphere where the meridional gradients in radiation are greatest. It is also of interest to note that the largest heat losses during winter are found not in the vicinity of the poles but near 65° latitude, which is possibly connected with the occurrence of ice-free water at those latitudes throughout the year so that heat losses can go on continuously.

The annual-mean net radiation flux at the earth's surface is presented in Fig. 6.12 as calculated by Budyko (1986) from Eq. (6.39) using some direct surface observations over land and oceans (see also Fig. 6.3). The radiation flux decreases with latitude from values of 160 to 180 W m^{-2} near the equator to values on the order of 20–40 W m^{-2} poleward of 60° latitude. Over most of the globe the net surface radiation is downward. However, over the polar regions in winter we may find a net radiation loss at the surface, when the solar influx tends to be very small or zero. In general, the values are higher over the oceans than over the continents at the same latitude. The highest values on the map are on the order of 180 W m^{-2} They occur in the intertropical regions over the oceans in agreement with the distribution of the total solar radiation absorbed in the atmosphere plus oceans shown in Fig. 6.10(b). Secondary equatorial maxima are found over the continents. The lowest values in the tropics occur over the deserts, which is to be expected from the high values of the surface albedo, the low values of cloudiness and humidity, and the high surface temperatures.

Zonal-mean radiation profiles at the top of the atmosphere based on the data from Campbell and Vonder Haar (1980) are shown in Figs. 6.13 and 6.14. The solar radiation available [Fig. 6.13(a)] exhibits a strong gradient in the winter hemisphere decreasing from a value of about 475 W m^{-2} in the subtropics of the summer hemisphere to a zero value at the winter pole, and only a weak gradient toward the summer pole. A considerable part of this radiation is reflected back to space as shown in Fig. 6.13(b). This is especially the case at high latitudes, where the albedo [see Fig. 6.14(a)] is very large ($> 70\%$) because of the greater angle of incidence of the incoming radiation and, to some extent, because of snow and ice coverage.

Finally, the curves for the absorbed solar radiation available for driving the earth's general circulation are given in Fig. 6.14(b). The main qualitative difference with the original solar energy curves in Fig. 6.13(a) is the decrease of available radiation over the summer pole, leading to an appreciable north–south gradient of absorbed solar radiation even in the summer hemisphere. The annual curves in Figs. 6.13(a) and 6.14(b) have practically the same shape with a shift of 100 W m^{-2} that is almost uniform over latitude. In analyzing the implications of these curves, it is good to recall that, for the globe as a whole, the annual average absorbed solar radiation is 238 W m^{-2} with an expected seasonal variation of about 8 W m^{-2} amplitude (see Fig. 6.8) due to the eccentricity of the earth's orbit around the sun.

The profiles of outgoing terrestrial radiation at the top of the atmosphere in Fig. 6.14(c) show a high plateau between about 30 °N and 30 °S with a slight dip over the ITCZ, mainly due to extensive cloudiness, and low values at high latitudes. The atmosphere over the Antarctic seems to lose less infrared radiation than the Arctic

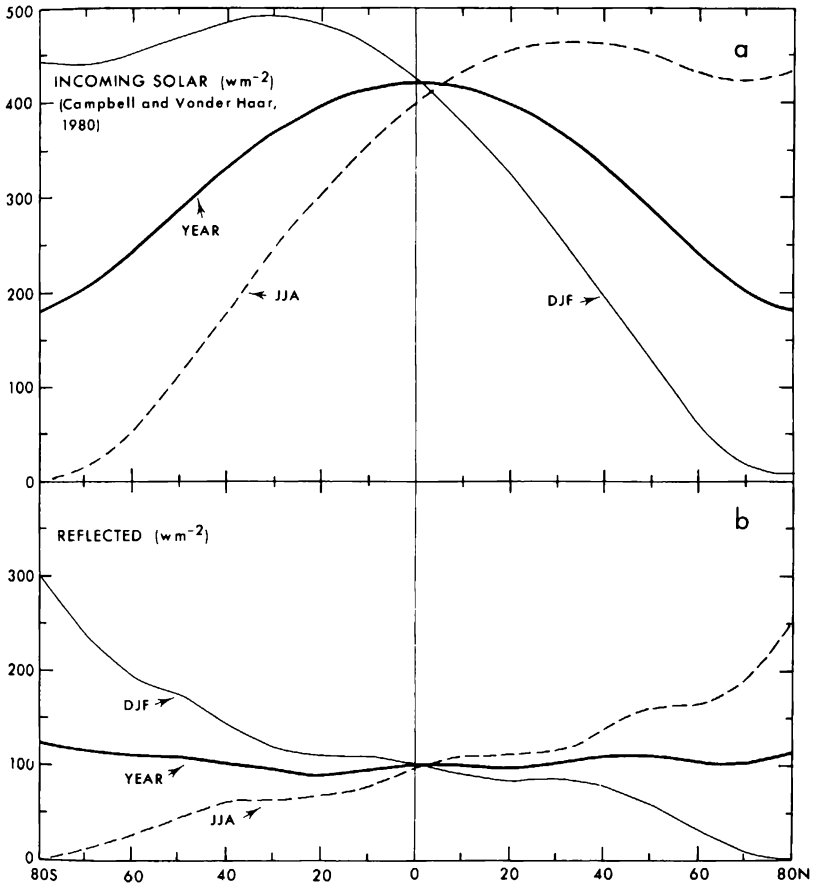

FIGURE 6.13. Meridional profiles of the zonal-mean incoming (a) and reflected solar radiation (b) at the top of the atmosphere in W m $^{-2}$ for annual, DJF, and JJA mean conditions (based on data from Campbell and Vonder Haar, 1980). No corrections were made to insure global radiation balance.

atmosphere, presumably because of the high ice cap in the Antarctic (Bowman, 1985; Nakamura and Oort, 1988). However, the north–south gradients in outgoing longwave radiation are always weak. The net meridional heating profiles given in Fig. 6.14(d) are obtained by subtracting the emitted terrestrial from the absorbed solar radiation profiles. The shape of the resulting profiles closely resembles the shape of the profiles of absorbed radiation although variations in cloudiness and surface albedo over deserts, forests, oceans, etc., also play a role in shaping these profiles. However, it is beyond the scope of the present book to further analyze these factors.

A synthesis of the hemispheric and global radiation components of the energy budget is presented in Table 6.2. The upper portion of the table gives the results without correction for global annual balance. It shows a net annual excess radiation

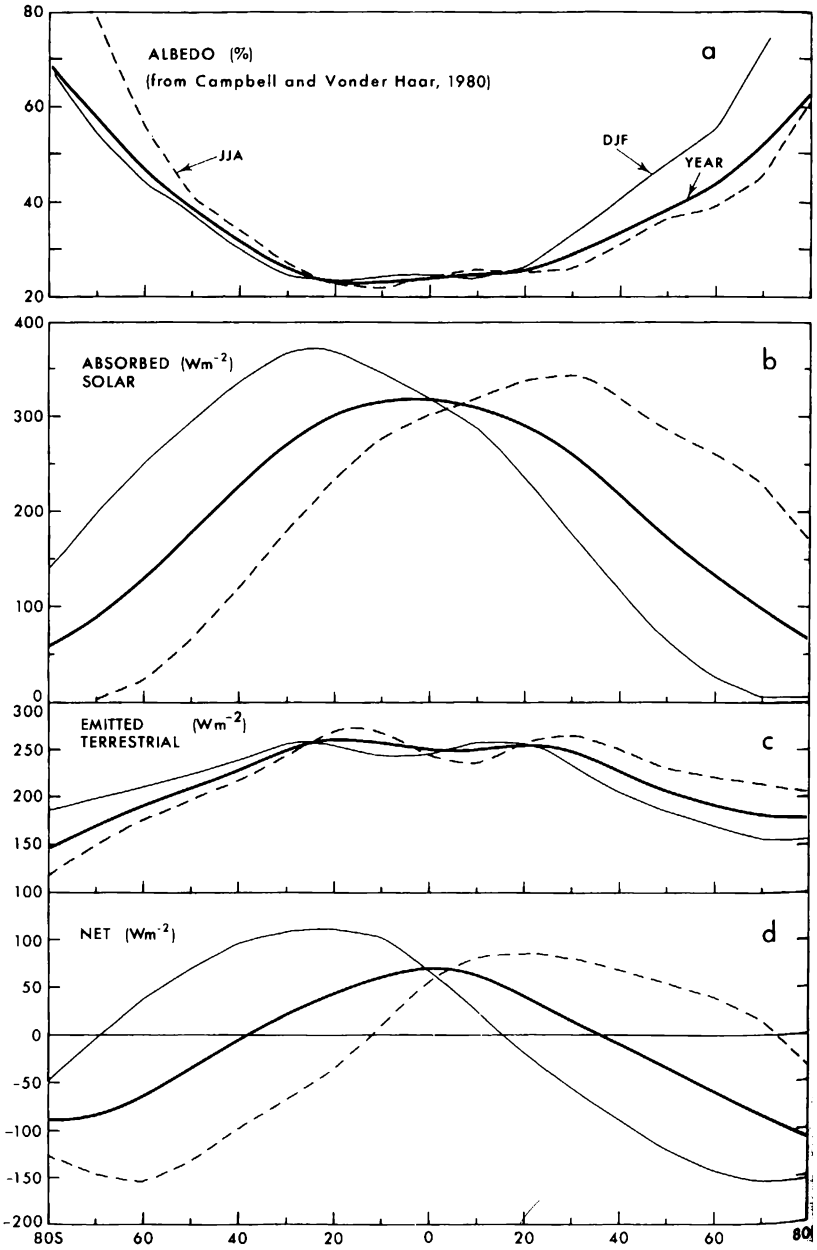

FIGURE 6.14. Meridional profiles of the zonal-mean albedo (a), absorbed solar radiation (b), emitted terrestrial radiation (c), and net radiation (d) at the top of the atmosphere for annual, DJF, and JJA mean conditions (based on data from Campbell and Vonder Haar, 1980). No corrections were made for global radiation balance.